Ecuaciones de Potencial y de Dirac para dispositivos quirales de grafeno

H. Torres-Silva[1]

[1] Instituto de Alta Investigación, Universidad de Tarapacá, Casilla 6-D, Arica, Chile.

htorres@uta.cl

Abstract

New electronic devices such as touch screens, flexible displays, printable electronics, solid-state lighting and thin film photovoltaics have led to a rapidly growing market for flexible transparent conductors. Recent advances in the synthesis and characterization of graphene indicate that it may be suitable for many electronic applications including as a transparent conductor.
The optimization of chiral graphene devices is performed using full wave analysis tools based on Method of Moments (MoM), and Finite Difference Time Domain (FDTD). Inclusion of the gauge condition gave rise to non-symmetric Newton-Raphson matrices, when solving non-linear electromagnetic problems. This can be repaired by the inclusion of a 'ghost' field that has no physical effects but results into non-singular and square Newton-Raphson matrices.
As application, we have calculated the influence of the optical effect (OE) on the chiral tunneling in graphene by using the FDTD method. We find that perfect tunneling can be strongly suppressed by the optically induced band mixing, even at large detuning. These properties might be useful in device applications, such as the fabrication of an optically controlled field-effect transistor that has ultrafast switching times and low power consumption.

---- *Keywords*: Chirality, potential equations, Dirac, waveguide, graphene.

Resumen

La optimización en el diseño de dispositivos quirales de grafeno se realiza mediante las herramientas del análisis de onda completa, basado en el Método de los Momentos (MoM) y en el Método de las Diferencias Finitas en el Dominio del Tiempo (FDTD). La inclusión de las condiciones de calibre, al resolver los problemas electromagnéticos no lineales, da lugar a la aparición de matrices no simétricas de Newton-Raphson. Como aplicación, se calcula la influencia del efecto óptico OE sobre el tunelamiento quiral en grafeno, usando el método FDTD. Se encuentra que el tunelamiento perfecto puede ser fuertemente suprimido por mezcla de banda inducida opticamente, aún con gran desintonía. Esas propiedades pueden ser útiles en aplicaciones con dispositivos quirales tales como la fabricación de un transistor por efecto de campo controlado que tiene tiempos de encendido-apagado ultrarrápidos y bajo consumo de potencia

---- *Palabras clave*: chiralidad, ecuaciones de potencial, Dirac, guías de ondas, grafeno

Introduction

Integrated Circuits: a Hierarchical Approach

Present-day integrated circuits are characterized by the down-scaling of device dimensions, the densification of device stacking as well as increased operation frequency. Furthermore, the integration of on-chip passive elements in the back-end process of the circuit designs a continuing activity. The density device stacking combined with a higher clock frequency leads to unprecedented design difficulties because one needs to keep parasitic couplings below prescribed threshold levels (design rules). On the other hand, the integration of on-chip passives requires a detailed knowledge of the characteristic parameters such as the capacitance, inductance and resistance. These global parameters can be regarded as effective parameters representing objects that are obtained from integrating a local, i.e. space-time dependent quantity. As such, these parameters will be sensitive to the frequency under consideration.

In order to arrive at a full chip design, a hierarchical approach is advocated. The design-rule checking is done by partitioning the design into blocks and within each block one may zoom in to the critical parts can usually be handled by lumped-element descriptions or transmission line theory. The critical paths are sometimes referred to as ‘tunnels’ [1-3].

At the deepest level, the simulation of the back-end structures should be done by a field-solver approach. However, the circumstances at this level are rather unconventional from a field-solvers point of view.

We will summarize here the specific difficulties that a field solver should be able to deal with Geometry [4]. The structures that appear at this level are often essentially three dimensional. As a consequence, transmission-line theory is not applicable. The patterns have a width and height of comparable size. Therefore, approaches that assume infinitely thin metallic layers are not justified from first principles. Metallic patterns [3] will have finite resistivity and therefore the currents will flow with different densities in the metallic parts. These currents distributions are further modified by the skin effect and proximity effects if the frequency increases.
Considering all the requirements listed above, we discuss in this paper a novel approach. Instead of building on existing approximation schemes derived from Maxwell’s equations, we choose to return to the Maxwell equations and to develop a solution scheme capable if dealing with the above problems. In addition it proves beneficial not only to return to the Maxwell equations, but also to carefully trace the physics that is hidden in the various symbols, In particular, the `physical` identification of the vector potential is crucial for a successful numerical implementation. There exists an intimate connection between differential geometry and electrodynamics that we have to exploit in order to perform this task.
On the other hand, Electrodynamics was discovered as a phenomenological theory. Starting from early experiments one arrived after considerable effort at Gauss’ law, Biot-Savart`s law and Faraday of induction. Only Maxwell’s law was obtained by theoretical reasoning and later experimentally confirmed by Hertz. Maxwell‘s great

achievement was later equalized by Einstein who proposed in the general theory of relativity that gravity ≡ curvature [5]. Ever since Einstein's achievement of describing gravity in terms of non-Euclidean geometry, theoretical physics has witnessed a stunning development. Based of geometrical reasoning resulting into the gauge theories, having a geometrical interpretations, very analogous to Einstein's theory of gravity. Electrodynamics is the low-energy limit of these gauge theories. Besides the aesthetic beauty that results from these insights, there is also pragmatic benefit. Solving electrodynamics problems on the computer, guided by the geometrical meaning of the variables is a decisive factor for the success of the calculation. This was already realized by Wilson [4] who initiated computer calculations on the quantum aspects of gauge theories. In order to perform computer calculations of the classical fields, geometry plays. An equally important role as will be shown here.

The classical fields ***E*** and **B** as well as the sources ρ and **J** are invariant under gauge transformations and therefore their underlying geometrical meaning is hidden. We may identify the proper geometric character for these variables, such as scalars (zero-forms), force fields (one-forms), (zero-forms), fluxes (two-forms) or volume densities (three-forms) as could be done for any other fluid dynamic system. This can be done without reference to the geometric nature of electrodynamics in the sense that ***E*** and ***B*** represent the curvature in the geometrical interpretation of electrodynamics. Therefore, in this paper we will consider the scalar potential and vector potential fields that do depend on gauge transformations and as such will give access to the geometry of electrodynamics. In this context we study the graphene physics, modeling the interaction of laser wave with the massles Dirac particles of the bidimensional graphene under chiral potential laser.

The geometrical interpretation of electrodynamics: Potential vector equation

Assuming $e^{j\omega t}$ time dependence, Maxwell's time-harmonic equations [5, 26] for isotropic, homogeneous, linear media are:

$$\nabla \times E = -j\omega B \tag{1}$$

$$\nabla \times H = j\omega D + J \tag{2}$$

$$\nabla \cdot B = 0 \tag{3}$$

$$\nabla \cdot D = \rho \tag{4}$$

Chirality is introduced into the theory by defining the following constitutive relations to describe the isotropic chiral medium [5]

$$D = \varepsilon E + \varepsilon T \nabla \times E \tag{5}$$

$$B = \mu H + \mu \nabla \times H \tag{6}$$

Where the chirality factor indicates the degree of chirality of the medium, and the ε y μ are permittivity and permeability of the chiral medium, respectively. Since D and E are polar vectors and B and H are axial vectors, it follows that ε and μ are true scalars and T is a pseudoscalar. This means that when the axes of a right-handed Cartesian coordinate system are reversed to form a left-handed Cartesian coordinate system, T changes in sign whereas ε and μ remain unchanged.

Let us assume vector-differential operator, ∇, is an ordinary vector and treat the divergence and curl operations in Equations (1) to (4) as ordinary scalar (dot) and vector

(cross) products, respectively. Equation (3) implies that ∇ is perpendicular to B and the vector $\nabla \times B$ must be perpendicular to both ∇ and B. Three transverse coordinate axes are chosen as ∇, from equation (1), $B = -\nabla \times E/(j\omega)$ and, $\nabla \times B/(j\omega\varepsilon\mu) = \nabla \times \nabla \times E/k^2$ where $k^2 = \omega^2\varepsilon\mu$. Since $\nabla \cdot B = 0$ always, this conditions will hold identically if B is expressed as the curl of a vector potential A since the divergence of the curl of a vector is identically zero. Thus

$$B = \nabla \times A \tag{7}$$

And A must be perpendicular to both ∇ and B and lie in ∇ and $\nabla \times B$ plane. However, A is not unique since only its components perpendicular to ∇ contribute to the cross product. Therefore, $\nabla \cdot A$, the component of A parallel to ∇, must be specified. The curl equation for E, as in Equation (1), and Equation (7) give $\nabla \times (E + j\omega A) = 0$ where the quantity in parentheses should be parallel to ∇ and the curl of the gradient of a scalar function ϕ is identically zero; so the general integral of the above equation is $E + j\omega A = -\nabla\phi$ or

$$E = -j\omega A - \nabla\phi \tag{8}$$

Substituting Equation (7) into Equation (6) we obtain

$$\nabla \times A = \mu H + \mu\nabla \times H \tag{9}$$

Substituting Equation (9) and Equation (5) into Equation (2) gives $\nabla \times \nabla \times A + j\frac{\omega\mu\varepsilon T}{1-k_o^2T^2}\nabla \times E = j\frac{\omega\mu\varepsilon}{1-k_o^2T^2}E - \frac{\omega^2\mu\varepsilon T}{1-k_o^2T^2}B + \frac{\mu}{1-k_o^2T^2}J$ placing the value of $\nabla \times E$ from equation (1) into the above equation $\nabla \times \nabla \times A + 2\frac{\mu\omega^2\varepsilon T}{1-k_o^2T^2}B = j\frac{\omega\mu\varepsilon}{1-k_o^2T^2}E + \frac{\mu}{1-k_o^2T^2}J$ using the vector identity $\nabla \times \nabla \times A = \nabla(\nabla \cdot A) - \nabla^2 A$ enables us to write the above equation as $\nabla^2 A + 2\frac{\omega^2\mu\varepsilon T}{1-k_o^2T^2}\nabla \times A = \nabla(\nabla \cdot A) - j\frac{\omega\mu\varepsilon}{1-k_o^2T^2}E - \frac{\mu}{1-k_o^2T^2}J$ and using Equation (8)

$$\nabla^2 A + \frac{k_0^2}{1-k_0^2T^2}A + 2\frac{\omega^2\mu\varepsilon T}{1-k_o^2T^2}(\nabla \times A) = \nabla(\nabla \cdot A - j\frac{\omega^2\mu\varepsilon T\phi}{1-k_o^2T^2}) - \frac{\mu}{1-k_o^2T^2}J \tag{10}$$

Implications form numerical simulations

In order to perform numerical computations starting from the fields $A_\mu = (\phi, \vec{A})$ it is necessary to introduce a discretization grid. The simulation of a finite space and/or space-time domain requires that each grid point is separated a finite distance from its neigh boring points. Than the differential operators that appear in the continuous field equations must be translate to the discretization grid by proper reference: to the geometrical meaning of the variables. The connections A_μ should be assigned to the links in the grid.

The geometrical interpretation suggests that the link assignment is the only correct scheme for solving chiral vector-potential field problems on the computer.

The numerical consequences of the above assignment will be considered in the following example, in which we will solve the steady-state equations $\nabla \times \vec{B} = \mu_0 \vec{J}$, $\vec{B} = \nabla \times (\vec{A} + T\nabla \times \vec{A})$,

$\vec{J} = \sigma \vec{E}$, $\vec{E} = -\nabla V - \frac{\partial(\vec{A} + T\nabla \times \vec{A})}{\partial t}$. The usual approach consists of substituting the second equation in to the first one, adopting the coulomb gauge $\nabla \vec{A} = 0$ and obtaining $\nabla^2(1-k_0^2T^2)\vec{A} + 2k_0^2T\nabla \times \vec{A} + k_0^2\vec{A} = -\mu_0\vec{J}$. Analytic solution schemes address this equation as a three-fold Poisson equation. This approach is usually sustained in numerical solution schemes, assigning the three components A_x, A_y, A_Z to the nodes of the discrete lattice. This approach is in conflict, with the geometrical interpretation of electrodynamics, since three scalar fields and the three components of a vector field are geometrically different objects.
We will now discretize the set of equations on a regular Cartesian grid having *N* nodes in each direction following our new approach. The total number of nodes in *D* dimensions is $M_{nodes} = N^D$ and the number of links in the lattice is $M_{links} = DN^D(1-\frac{1}{N})$.
As far as the description of the electromagnetic field is concerned, the counting of unknowns for the full lattice results into M_{links} M_{links} variables (A_{ij}) for the links, and M_{nodes} variables (V_i) for the nodes. Since each link (node) gives rise to one equation, the naive counting is consistent. However, we have not yet implemented the gauge condition. The conventional Coulomb gauge $\nabla \vec{A} = 0$, constrains the link degrees of freedom and therefore not all link fields are independent. There are $3N^3(1-\frac{1}{N})$ link variables and $3N^3(1-\frac{1}{N}) + N^3$ equations, including the constraints. As a consequence, at first sight it seems that we are confronted with an over determined system of equation, since each node provides an extra equation for $\vec{A}$. However, the translation of the Maxwell-Ampere equation on the lattice leads to a singular matrix, i.e. not all rows are independent. The rank of the corresponding matrix is $3N^3(1-\frac{1}{N})$, whereas there are $3N^3(1-\frac{1}{N}) + N^3$ rows and $3N^3(1-\frac{1}{N})$ columns. Such a situation is highly inconvenient for solving non-linear systems of equations, where the non-linearity stems from the source terms being explicitly dependent on the fields moreover, the application of the Newton-Raphson method requires that the matrices in the Newton equation be non-singular and square. In Fact, the non-singular square form of the Newton matrix can be recovered by introducing the more general gauge $\nabla \vec{A} + \nabla^2\chi = 0$, where an additional scalar field *x*, i.e. one unknown per node, is included. In this way the number of unknowns and the number of equations match again. In the continuum limit (N $\to \infty$), the field *x* and one component of $\vec{A}$ can be eliminated.
Though being irrelevant for theoretical understanding, the auxiliary field *x* is essential for obtaining numerical stability on a discrete, finite lattice.

In other words, our specific gauge solely serves as a tool to obtain a discretization scheme that generates a regular Newton-Raphson matrix.
To summarize, instead of solving the problem

$$\nabla \times \nabla \times (1-k_0^2T^2)\vec{A} - 2k_0^2T\nabla \times \vec{A} - k_0^2\vec{A} = \mu_0\vec{J}, \quad \nabla \vec{A} + \nabla^2\chi = 0 \tag{13}$$

we solve the equivalent system of equations

$$\nabla\times\nabla\times(1-k_0^2T^2)\vec{A}-2k_0^2T\nabla\times\vec{A}-k_0^2\vec{A}-\gamma\nabla\chi=\mu_0\vec{J}(\vec{A}) \quad , \quad \nabla\vec{A}=0$$

(14)

The equivalence of both sets of equations (13) and (14) is because physical equivalence is guaranteed provided that $\nabla\chi$ does not lead to an additional current source. Therefore, it is required that $\nabla\chi = 0$. In fact, acting with the divergence operator on the first equation of (14) gives Laplace's equation for χ . The solution of the Laplace's equation is identically cero if the solution vanishes at boundary. We achieved to implement the gauge condition resulting into a unique solution and simultaneously to arrive at a systems containing the same number of equation and variables. Hence a regular square Newton-Raphson matrix is obtained at each stage of the numerical solution scheme that solves the full set of non-linear equations. [6,7]

Discretized operators

Integrated over a test volume ΔVi surrounding a node *i*, the divergence operator, acting on vector potential *A,* can be discretized as a combination of 6 neigh boring links.

$$\int_{\Delta V_i}(1-k_0^2T^2)\nabla\vec{A}d\tau=(1-k_0^2T^2)(\int_{\partial(\Delta V_i)}\vec{A}d\vec{S}\approx\sum_k^5 S_{ik}A_{ik})$$

The symbol ~ represents the conversion to the grid formulation and ∂ (ΔVi) denotes the boundary of ΔVi [6].

The curl-curl operator can be discretized for a link *ij* using a combination of 12 neigh boring links and the link *ij* itself. As indicated in Fig. 1, the field B_i in the center of the 'wing' i, can be constructed by taking the circulation of the vector potential A around the wing *i (i* = 1, 4)

$$B_iS_i\approx(1-k_0^2T^2)(\sum_{j=1}^3 A_{ij}h_{ij}+A_0h_0)$$

Where h_α is the length of the corresponding link α . Integration over a surface S_{ij} S_{ij} perpendicular to the link *ij* yields a linear combination of different A_{ij} , the coefficient of which are denoted by A_{ij} .

$$\int_{\Delta S_{ij}}(1-k_0^2T^2)\nabla\times\nabla\times\vec{A}d\vec{S}=\int_{\partial(\Delta S_{ij})}(1-k_0^2T^2)\nabla\times\vec{A}d\vec{r}=(1-k_0^2T^2)(\Lambda_{ij}A_{ij}+\sum_{kl}^{12}\Lambda_{ij}^{kl}A_{kl})$$

The influence of the optical laser on chiral tunneling in graphene

Graphene has attracted much attention due to its remarkable electronic properties [8–10]. The low-energy quasiparticles, which have linear dispersion and nontrivial topological structure in their wave function, can be described by using a Dirac-like equation. This unique band structure of graphene leads to many important potential applications in nanoelectronics [11–16].

One of the peculiar transport phenomena in graphene is the chiral tunneling [11, 12, 17]. In single layer graphene a perfect transmission through a potential barrier in the normal direction is expected. This unique tunneling effect can be explained by the chirality of the Dirac electrons within each valley, which prevents backscattering in general. This kind of reflectionless transmission is independent of the strength of the potential, which limits the development of graphene-based field-effect transistors (FET) [11]. The perfect transmission can be suppressed effectively when the chiral symmetry of the Dirac electrons is broken. The intense optical field can also break the chiral symmetry of Dirac electrons in graphene, e.g., In [18] we can see that when the n-p Junctions in graphene is irradiated by an electromagnetic field in the resonant condition, the quasiparticle transmission is suppressed. The optical field control on carrier transport offers several advantages. Optical fields can control not only the charge carriers but also the spin carriers, especially which can be performed over femtosecond time scale. Another fundamental method of optical control is the optical effect (OE). The OE in traditional semiconductors is due to a dynamical coupling of excitonic states by an intense laser field. The OE has shown many useful applications in optoelectronics and spintronics [19-25].

In graphene, the valence band and conduction band states can also mix strongly via OE. Thus the chirality of Dirac electrons will be completely changed, or even disappear. Unlike the resonant case [18], in OE the coherent excitons are virtual excitons, which exist only when the optical field is present. Thus the light-induced shift lasts only for the duration of the pump pulse, which allows for optical gates that might only exist for femtoseconds. Furthermore, since there is no real absorption in the nonresonant case, the absorption of photons is quite small and low power consumption is expected.

In this section, we study the tunneling rate of Dirac electrons in graphene through a barrier with an intense electromagnetic field. We consider a rectangular potential barrier with height V_0, width D in the X direction, and infinite length in the Y direction. The Fermi level lies in the valence band in the barrier region and in the conduction band outside the barrier. The gray filled areas indicate the occupied states. The optical field is propagated perpendicular to the layer surface and is circulary polarized along the Z,Y direction with a detuning $\Delta_0 = 2E_b - \hbar\omega$.

We choose $\Delta_0 > 0$ to ensure that there is no interband absorption inside the barrier. Meanwhile, $2E_k >> \hbar\omega$ is used to guarantee that the influence of the optical field outside the barrier can be neglected.

Since the Coulomb interaction between electrons and holes in OE is negligible when the detuning is large [21, 24], we did not take into account the electron-hole Coulomb interaction or many body effect in our calculation. Thus, neglecting the scattering between different valleys, the scattering process of Dirac electrons in K point is described by the time-dependent Dirac equation

$$i\hbar\frac{\partial}{\partial t}\psi(r,t) = \left[H_0 + V_0 I + H_{\text{int}}\right]\psi(r,t), \tag{15}$$

where $\psi(r,t) = \left[\phi_A(r,t), \phi_B(r,t)\right]$ is the wave function, $H_0 = v_F\sigma\cdot p = -i\hbar v_F\sigma\cdot\nabla$ is the unperturbed Dirac Hamiltonian, $\sigma = (\sigma_x\sigma_y)$ are the Pauli matrices, $v_F \approx 10^6 ms^{-1}$ is the

Fermi velocity, $V_0(r)$ is the height of the potential barrier, I is the unit matrix, and H_{int} is the interaction Hamiltonian. H_{int} can write as [27]

$$H_{\text{int}} = -ev_F\left[A(x,t)\sigma_x + A(y,t)\sigma_y\right] = \begin{pmatrix} 0 & H_{12} \\ H_{21} & 0 \end{pmatrix} \tag{16}$$

where e is the electron charge and $\left[A(x,t), A(y,t)\right] = \left[A_x e^{i\omega t}, A_y e^{i\omega t}\right]$ and $|A_x| = |A_y|$ are the chiral vector potentials of the electromagnetic field obtained from the solution of equations (13, 14) with $1 - k_0 T = \alpha$ where $\alpha = e^2 / (4\pi\varepsilon_0 hc)$ is the fine structure constant. When the Dirac electrons is incident on the barrier perpendicularly, we can rewrite Eq. (15) as a set of partial differential equations

$$i\frac{\partial}{\partial t}\phi_A(x,t) = -iv_F\frac{\partial}{\partial x}\phi_B(x,t) + V_0\phi_A(x,t) + H_{12}(t)\phi_B(x,t) \tag{17}$$

$$i\frac{\partial}{\partial t}\phi_B(x,t) = -iv_F\frac{\partial}{\partial x}\phi_A(x,t) + V_0\phi_B(x,t) + H_{21}(t)\phi_A(x,t) \tag{18}$$

Since the tunneling time is sub-picosecond and the potential $H_{12}(t)$ and $H_{21}(t)$ vary as fast as the frequency of incident light beams, this scattering process is strongly time-dependent. In order to study such a strongly time-dependent scattering process, we employ the finite- difference time-domain (FDTD) method to solve Eq. (17) and Eq. (18) numerically in the time-domain [25]. In the traditional FDTD method, the Maxwell's equations are discretized by using central-difference approximations of the space and time partial derivatives. As a time-domain technique, the FDTD method can demonstrate the propagation of electromagnetic fields through a model in real time. Similar to the discretization of Maxwell's equations in FDTD, we denote a grid point of the space and time as $(i,k) = (i\Delta x, k\Delta t)$ [24, 25]. For the nodal variables we can apply the usual Lee discretization method in 2-D systems and $k_0^2 T^2 \ll 1$.(Figure 1)

Figure 1: Lee discretization method . Here, $H_x = (\nabla \times \vec{A})_x$ $E_x = -(\partial(1 + T\nabla\times)\vec{A}/\partial t)_x$ and so on… with $\vec{J} = 0$. See equations (13, 14)

For the any function of space and time $F(i\Delta x, k\Delta t) = F^k(i)$.
The first order in time or space partial differential can be expressed as

$$\left(\frac{\partial}{\partial x}F(x,t)\right)_{x=i\Delta x} \approx \frac{F^k(i+1/2) - F^k(i-1/2)}{\Delta x} \tag{19}$$

$$\left(\frac{\partial}{\partial t}F(x,t)\right)_{t=k\Delta t} \approx \frac{F^{(k+1/2}(i) - F^{(k-1/2}(i)}{\Delta t} \tag{20}$$

Thus the Eq. (17) and Eq. (18) can be replaced by a finite set of finite differential equations

$$\phi_A^{k+1/2}(i)\left[\frac{1}{\Delta t}-\frac{V_0(i)}{2i}\right]=\left[\frac{1}{\Delta t}+\frac{V_0(i)}{2i}\right]\phi_A^{k-1/2}(i)-\left[\frac{v_F}{\Delta x}-\frac{V_{12}^k(i+1/2)}{2i}\right]\phi_B^{k}(i+1/2)$$
$$+\left[\frac{v_F}{\Delta x}+\frac{V_{12}^k(i-1/2)}{2i}\right]\phi_B^{k}(i-1/2) \qquad (21a)$$

$$\phi_B^{k+1}(i+1/2)\left[\frac{1}{\Delta t}-\frac{V_0(i+1/2)}{2i}\right]=\left[\frac{1}{\Delta t}+\frac{V_0(i+1/2)}{2i}\right]\phi_B^{k}(i+1/2)$$
$$-\left[\frac{v_F}{\Delta x}-\frac{V_{12}^{k+1/2}(i+1)}{2i}\right]\phi_A^{k}(i+1/2)+\left[\frac{v_F}{\Delta x}+\frac{V_{12}^{k+1/2}(i)}{2i}\right]\phi_A^{k+1/2}(i) \qquad (21b)$$

For computational stability, the space increment Δx and the time increment Δt need to satisfy the relation $\Delta x > v_F \Delta t$ [25, 26]. Furthermore, the space increment Δx must far smaller than the wavelength of electrons $\Delta x < \lambda_e / 10$, and the time increment Δt must be far smaller than the period of the electromagnetic field T_l.

At the boundary B_a, one-dimensional Mur absorbing boundary conditions are used [24, 25]. At the input boundary B_{in}, a Gaussian electronic wave packet is injected

$$\phi_A = \phi_B = \frac{1}{\sqrt{2}}\exp(-\frac{4\pi(t-t_0)^2}{\tau_G^2}), \qquad (22)$$

where t_0 and τ_G denote the peak position and the pulse width, respectively.

Thus, by solving Eq. (21a) and Eq. (21b) directly in the time domain we can demonstrate the propagation of a wave packet through a barrier in real time. Numerical simulations are shown in Fig. 2. The following parameters are used in our calculation: the peak position t_0 = 1.5 ps, the pulse width τ_G = 1.0 ps, the space increment Δx = 0.1 nm, the time increment $\Delta t = 5\times10^{-5}\, ps$, and the height of the potential barrier V_0 = 500 meV.

When there is no pump beams, a perfect chiral tunneling can be found [see Fig. 2(a)]. This result is consistent with that of Geim et al. [11]. But when the sample is irradiated by an intense non resonant laser beam, a reflected wave packet appears [see Fig. 2(d)]. The perfect transmission is suppressed. By analyzing the transmitted wave packet and the reflected wave packet, we can obtain the tunneling rate.

To explain the suppression of chiral tunneling, we first investigate the OE in the barrier within a rotating wave approximation [25]. Figure 2(a) shows the renormalized band as a function of momentum k with intensity $I_\omega = 3MW/cm^2$.

FIG. 2: (a) Numerical simulations of a wave packet given by $N = |\phi_A|^2 + |\phi_B|^2$, tunneling through a barrier without pump beams. Figures (b)-(d) show the time sequence of a wave packet tunneling through a barrier with pump intensity $I_\omega = 3MW/cm^2$, $\Delta_0 = 5\text{meV}$, and D = 350 nm. The light grey shows the barrier area.

Here we make $\pm k_0 T \; \square \; 1+\alpha$, where $\alpha = e^2/(4\pi\varepsilon_0 \square c)$ is the fine structure constant. Without external beams, (fig. 2 (a)), we verify the known results on chiral tunnelling [11]. Figures (b)-(d) show the time sequence of a wave packet tunneling through a barrier with pump intensity $I_\omega = 3MW/cm^2$, $\Delta_0 = 5\text{meV}$, and D = 350 nm.

Figure 3 Left: The reflectance R(red circles) and the transmittance T (black squares) of the barrier as a function of the detuning for $I_\omega = 3MW/cm^2$ and D = 350 nm. Right: The transmittance versus $I_\omega(MW/cm^2)$ Having D as parameter. Here, $k_0^2 T^2 \approx 1$.

Under intense light beams, the dressed states are strongly mixed with valence states and conduction states. Therefore, the chiral symmetry of Dirac electrons in graphene can be broken. For instance, at very small detuning, the wave functions of these dressed states can be approximately written as the superposition of unperturbed conduction and valence wave function. These dressed states are not the eigenstates of the helicity operator. The chiral symmetry is broken and perfect chiral tunneling is strongly suppressed. Numerical results are shown in Fig. 3(left) with pump intensity $I_\omega = 3MW/cm^2$ and D = 350 nm. From Fig. 3(left) we can find that the transmission is strongly suppressed, even with laser detuning (e.g., Δ_0 = 10 meV, the transmittance is about 0.03).

Figure 3 left, show that the reflectance decreases, and the transmittance increases as Δ_0 increases. The strong laser field can enhance band mixing and reduce the transmittance. If D increases we can see that the wide barrier can prolong the interaction time between electrons and photons, reduce the tunneling rate, and lower the threshold of the pump laser power (Figure 3 right).

In conclusion, we have calculated the influence of the OE on the chiral tunneling in graphene by using the FDTD method. We find that perfect tunneling can be strongly suppressed by the optically induced band mixing, even at large detuning. These properties might be useful in device applications, such as the fabrication of an optically controlled field-effect transistor that has ultrafast switching times and low power consumption.

5 Conclusions

We reviewed the geometrical aspects of electromagnetic field variables. Vector potentials are 1-forms.The vector potential need to be assigned to the links of the grid. Inclusion of the gauge condition gives rise to non-symmetric Newton-Raphson matrices, when solving non-linear electromagnetic problems. This can be repaired by the inclusion of a ‘ghost’

field that has no physical effects but results into non-singular and square Newton-Raphson matrices. The proposed potential formulation in terms of the vector field $\boldsymbol{A}$ and the ghost field x, is a viable method to solve the Maxwell field problem in graphene systems.
The influences of intense coherent laser fields on the transport properties of a single layer graphene are investigated by solving the time-dependent Dirac equation numerically. Under an intense laser field, the valence band and conduction band states mix via the optical effect. The chiral symmetry of Dirac electrons is broken and the perfect chiral tunneling is strongly suppressed. These properties might be useful in the fabrication of an optically controlled field-effect transistor

References

1. R. Shimano, H. Nishimura and T. Sato, "Frequency Tunable Circular Polarization Control of Terahertz Radiation". *Jpn. J. Appl.Phys*. Vol. 44, L676. 2005.
2. E. Castro-Camus, J. Lloyd-Hughes, M. B. Johnston, M. D. Fraser, H. H. Tan, and C. Jagadish, "Polarization-sensitive terahertz detection by multicontact photoconductive receivers," *Appl. Phys. Lett*. **86**, 254102 (2005).
3. Walker M.G. Modelling the wiring of deep submicron IC. *IEEE Spectrum* 2000; March edition
4. Wilson K, Confinement of Quarks. *Phys. Rev*. 1974; D10: 2445-2459
5. H. Torres-Silva, The New unification of gravitation and Electromagnetism, ISBN 978-956-332- 973-5. First Ed. 2011.
6. Meuris P., Schoenmaker W., Magnus W. Strategy for Electromagnetic Interconnect Modelling. *IEEE Trans*. On CAD 2000; Vol. 20 Nº 6.
7. J. B. Pendry, *Contemporary Physics*, Vol. 45 pp.191-202, (2004).
8. K. S. Novoselov, A. K. Geim, S. V. Morozov, D. Jiang, Y. Zhang, S. V. Dubonos, I. V. Grigorieva, A. A. Firsov, *Science* 306, 666 (2004).
9. K. S. Novoselov, A. K. Geim, S. V. Morozov, D. Jiang, M. I. Katsnelson, I. V. Grigorieva, S. V. Dubonos, A. A. Firsov, *Nature* 438, 197 (2005.

10. A. H. Castro Neto, F. Guinea, N. M. R. Peres, K. S. Novoselov, and A. K. Geim, *Rev. Mod. Phys*. 81, 109 (2009).

11. M. I. Katsnelson, K. S. Novoselov, and A. K. Geim, *Nature Physics* 2, 620 (2006).

12. V. V. Cheianov, V. Fal'ko, and B. L. Altshuler, *Science* 315, 1252 (2007).

13. Z. Z. Zhang, K. Chang, and K. S. Chan, *Appl. Phys. Lett*. 93, 062106 (2008).

14. V. H. Nguyen, A. Bournel, V. L. Nguyen, and P. Dollfus, *Appl. Phys. Lett*. 95, 232115 (2009).

15. P. Michetti, M. Cheli, and G. Iannacconea, *Appl. Phys. Lett*. 96, 133508 (2010).

16. E. Prada, P. San-Jose, and H. Schomerus, *Phys. Rev*. B 80, 245414 (2009).

17. W.-R. Hannes and M. Titov, *Europhysics Letters* 89, 47007 (2010).

18. M. V. Fistul and K. B. Efetov, *Phys. Rev. Lett*. 98, 256803 (2007).

19. C. E. Pryor and M. E. Flatt´e, *Appl. Phys. Lett*. 88, 233108 (2006).

20. S. Sanchez, C. De Matos, and M. Pugnet, *Appl. Phys. Lett*. 89, 263510 (2006).

21. W. Yao, A. H. MacDonald, and Q. Niu, *Phys. Rev. Lett*. 99, 047401 (2007).

22. J. T. Liu, F. H. Su, and H. Wang, *Phys. Rev. B* 80, 113302 (2009).

23. K. S. Yee, *IEEE Transactions on Antennas and Propagation*, 14 302 (1966).

24. G. Mur, *IEEE Transactions on Electromagnetic Compatibility* EMC-23, 377 (1981).

25. Jiang –Tao Ling, Fu-Hai Su, Hai Huang, Xin Hua-Deng, Arxiv:1007.3430v3

26. H. Torres-Silva, *Ingeniare* Vol. 16, pp. 91, (2008).

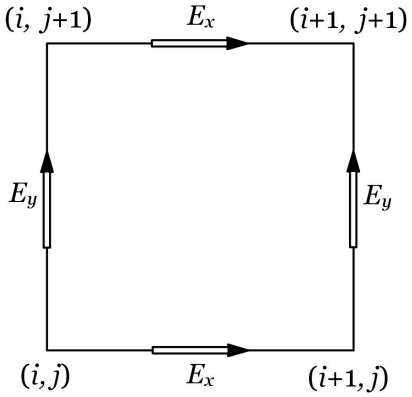

Figure 1: Lee discretization method . Here, $H_x = (\nabla \times \vec{A})_x$ $E_x = -(\partial(1+T\nabla\times)\vec{A}/\partial t)_x$ and so on… with $\vec{J} = 0$. See equations (13, 14)

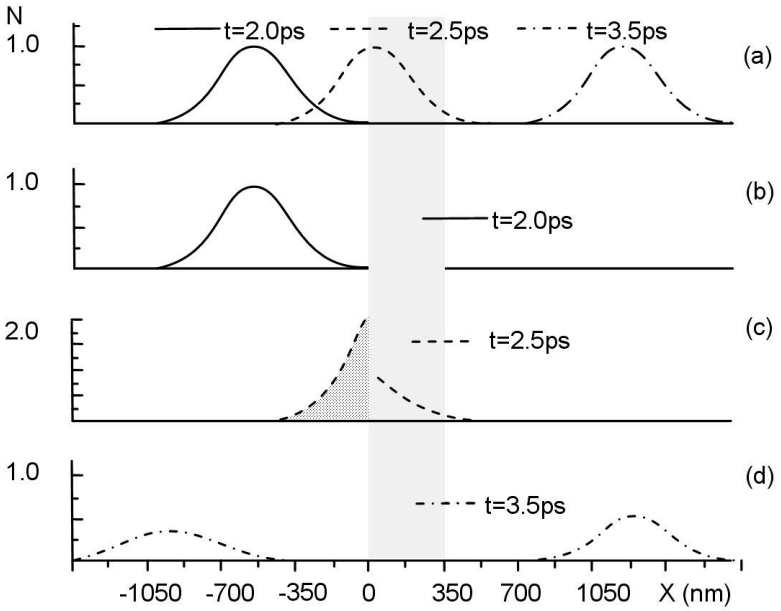

FIG. 2: (a) Numerical simulations of a wave packet given by $N = |\phi_A|^2 + |\phi_B|^2$, tunneling through a barrier without pump beams. Figures (b)-(d) show the time sequence of a wave packet tunneling through a barrier with pump intensity $I_\omega = 3MW/cm^2$, $\Delta_0 = 5\text{meV}$, and D = 350 nm. The light grey shows the barrier area.

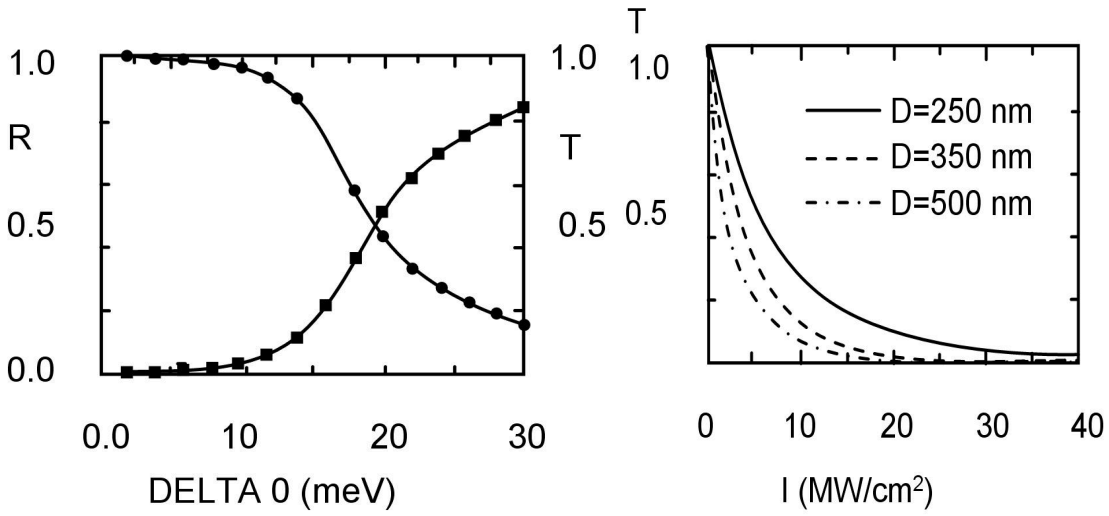

Figure 3 Left: The reflectance R(red circles) and the transmittance T (black squares) of the barrier as a function of the detuning for $I_\omega = 3MW/cm^2$ and D = 350 nm. Right: The transmittance versus $I_\omega(MW/cm^2)$ Having D as parameter. Here, $k_0^2T^2 \approx 1$.